Tracking metabolites at single-cell resolution reveals metabolic dynamics during plant mitosis

Okubo-Kurihara, E.; Ali, A.M.A.M.; Hiramoto, M.; Kurihara, Y.; Abouleila, Y.A.M.I.; Abdelazem, E.M.R.; ... ; Matsui, M.

https://doi.org/10.1093/plphys/kiac093 PLANT PHYSIOLOGY 2022: 189: 459–464

Plant Physiology®

Letter

Tracking metabolites at single-cell resolution reveals metabolic dynamics during plant mitosis

Emiko Okubo-Kurihara ,[1] Ahmed Ali ,[2,3] Mika Hiramoto,[1,4] Yukio Kurihara ,[1] Yasmine Abouleila ,[2,3] Eman Muhammad Abdelazem ,[2] Takayuki Kawai ,[3,5] Yuko Makita ,[1] Mika Kawashima,[1,‡] Tsuyoshi Esaki ,[6] Hiroaki Shimada ,[4] Tetsuya Mori ,[1] Masami Yokota Hirai ,[1] Takumi Higaki ,[7] Seiichiro Hasezawa,[8] Yoshihiro Shimizu ,[3] Tsutomu Masujima[3,‡] and Minami Matsui [1,*,†]

1 RIKEN Center for Sustainable Resource Science, Kanagawa, 230-0045, Japan
2 Division of Biopharmaceutics, LACDR, Leiden University, Leiden, The Netherlands
3 RIKEN Center for Biosystems Dynamics Research, Osaka, 565-0874, Japan
4 Faculty of Industrial Science and Technology, Tokyo University of Science, Tokyo, 125-8585, Japan
5 Graduate School of Science, Kyushu University, Fukuoka, 819-0395, Japan
6 The Center for Data Science Education and Research, Shiga University, Shiga, 522-0069, Japan
7 Department of Biological Sciences, Graduate School of Science and Technology, Kumamoto University, Kumamoto, 860-8555, Japan
8 Graduate School of Science and Engineering, Hosei University, Tokyo, 184-8584, Japan

*Author for correspondence: minami@riken.jp
These authors contributed equally (E.O.K. and A.A.).
†Senior author.
‡These authors passed away before this article was submitted.

E.O.K. and A.A. were responsible for the organization and coordination of the trial. E.O.K., M.H., A.A., Y.A., T.K., and Y.K. carried out the experiments and E.O.K., A.A., Y.A., M.H., Y.K., Y.M., E.M.A., and M.K. performed the data analysis of the single-cell metabolome. A.A. and T.E. contributed to the single-cell MS analysis tools. Te.M. and M.Y.H. annotated the metabolome data. T.H. and S.H. developed the BY-HR cells. All authors contributed to the writing of the final manuscript. M.M., Y.S., H.S., and Ts.M. were the principal investigators and responsible for the management of the trial.
The author responsible for distribution of materials integral to the findings presented in this article in accordance with the policy described in the Instructions for Authors (https://academic.oup.com/plphys) is: Minami Matsui (minami@riken.jp).

Dear Editor,

Mitosis is a dynamic process involving a cell duplicating into two daughter cells that must be tightly regulated at the molecular level. Mitosis consists of four successive sub-phases: prophase, metaphase, anaphase, and telophase. Each mitotic sub-phase is described according to the state of the chromosomes (Alberts et al., 1994), but not much attention has been paid to the metabolic profile of each phase. In this study, we attempted to gain more insight into the mitotic intracellular metabolic behavior using imaging and mass spectrometry-based single-cell analysis.

To precisely extract single cells of each mitotic sub-phase, we established tobacco BY-HR cells (the BY-2 cell line-expressing *histone 2B-RFP*) to visualize the chromosomal status at each mitotic sub-phase (Supplemental Figure S1). Little difference was observed in the period of cell division, or the growth rate of these cells compared with the wild-type (Supplemental Figure S1). This research aims to investigate metabolic changes in each sub-phase on the single-cell level, as well as determine very long-chain fatty acids (VLCFAs) accumulation during mitosis. We prepared protoplasts from the BY-HR cells and manually isolated a single protoplast undergoing prophase, metaphase, anaphase, or telophase using a micromanipulator attached to a sampling capillary under fluorescent microscopic observation (Figure 1A).

To track the metabolite profile of each mitotic sub-phase, we measured the isolated cells by live single-cell-mass spectrometry (LSC-MS). This technology enables the detection of metabolites in a live single cell with high sensitivity and selectivity (Tejedor et al., 2012; Fujii et al., 2015; Abouleila

Received November 23, 2021. Accepted January 23, 2022. Advance access publication March 18, 2022

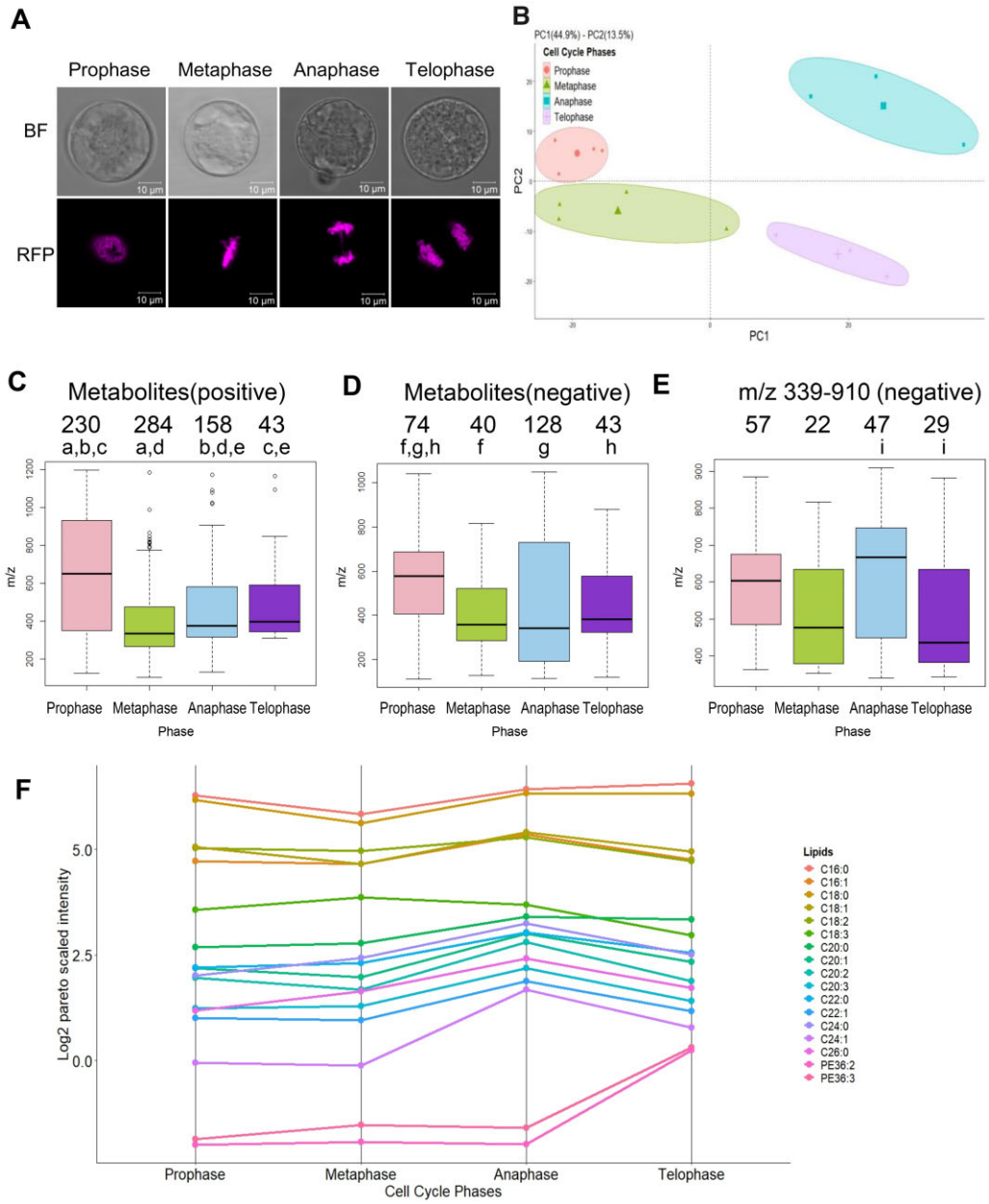

Figure 1 Changes in metabolite accumulation during mitotic progression. A, Chromosomal state of BY-HR protoplasts in different mitotic sub-phases. BF: bright field. RFP: histone 2B-RFP. B, Score plot of PCA-DA based on metabolomics data of the mitotic sub-phase. Each data point corresponds to a single-cell sample. Symbols of the same size represent each single cell sample, and the larger symbol in the middle of the ellipse is the average of the other points. The contribution ratio of PC1 is 44.9% and PC2 is 13.5%. C, Distribution of phase-specific peaks of significant metabolites detected in positive mode. a, b, c, d, and e indicate a significant difference in distribution between the sub-phases. The lower end of the whiskers shows the minimum value and the upper end of the whiskers shows the maximum value. The lower bottom of the box represents the 25 percentile of data from the smallest, the horizontal line in the box the median and the upper bottom the 75th percentile. Some of the points are outliers. The number shown above the box and whisker diagrams is the number of time-specific metabolites. a, b, c, and d: $P < 0.005$ (ANOVA-Tukey test), e: $P < 0.02$ (ANOVA-Tukey test), (D) all metabolites detected in negative mode and (E) m/z 339–910 lipids in negative mode. f, g, h, and i indicate a significant difference in distribution between the sub-phases. g, h, and i: $P < 0.03$ (ANOVA-Tukey test), f: $P < 0.005$. F, The median intensity of each VLCFA was plotted in a parallel coordinators plot. The figure shows all the lipids mentioned in the paper by Bach et al. (2011) Each m/z of the VLCFAs was calculated using lipidmaps database (https://www.lipidmaps.org/), and it was matched to the dataset. The lipids that had a positive match were plotted, where the median intensity of each lipid for each phenotype is plotted.

et al., 2019; Ali et al., 2019). Single-cell analysis sidesteps the limitations of measurements taken by averaging a population, and results in precise metabolic profile of each mitotic sub-phase. This single-cell metabolome analysis was done for a minimum of three single cells in each sub-phase (Supplemental Figure S2).

Cells of each sub-phase clustered close to each other and cells of different sub-phases clustered separately (Figure 1B), suggesting that each mitotic sub-phase has its own specific metabolic components. To investigate this observation further, the significant peaks ($P < 0.05$) for each sub-group were plotted in a heatmap, where different patterns among the four sub-phases were also observed (Supplemental Figure S3). These results suggest that during mitosis, regulation of metabolites is dependent on the sub-phase.

To dissect the metabolic features in each sub-phase, annotation of the unique sub-phase peaks was carried out using their exact masses and isotopic patterns. In prophase, metaphase, anaphase, and telophase, 230, 284, 158, and 43 phase-specific metabolites ($P < 0.05$) were found in positive mode, and 74, 40, 128, and 43 phase-specific metabolites ($P < 0.05$) were present in negative mode, respectively (Figure 1, C and D; Supplemental Figures S1 and S2). Peak annotation was done using two lists of *Nicotiana* metabolites (KNApSAcK_Nicotiana and DNP_Nicotiana) corresponding to metabolite information extracted with the word "Nicotiana" from the database KNApSAcK (Afendi et al., 2011) and the Dictionary of Natural Products (https://dnp.chemnetbase.com/faces/chemical/ChemicalSearch.xhtml) as a permissible range of 0.01 Da (Supplemental Data Sets 1 and 2). Of these, only those with peaks and annotations were extracted and listed in Supplemental Tables S1 and S2. In positive and negative modes, there was a high degree of heterogeneity in the distribution of individual metabolites along the *m/z* axis in each phase (Figure 1, C and D). These results are characterized by a pattern of metabolites in each phase, and changes in this pattern may be important for the progression of mitotic sub-phases.

Next, to extract the salient features, we focused on the lipidomic profiles. In HeLa cells, dynamic changes in lipid composition and localization regulate cell division and midbodies (Atilla-Gokcumen et al., 2014). In plants, lipids are also involved in membranes and membrane trafficking, important in the formation and disappearance of the phragmoplast and in cell plate assembly during cell division (Caillaud, 2019). We focused on VLCFAs, which are defined as having 18–22 or more carbon atoms, and found differences between the sub-phases. In this article, we defined VLCFA as C22 or higher based on Kihara's (2012) paper, and calculated the corresponding molecular weight, which was 339–910 at *m/z*. Therefore, we investigated the region of *m/z* 339–910 in negative mode containing the expected VLCFA. Our results show that 57, 22, 47, and 29 phase-specific VLCFA (corresponding to *m/z* 339–910) metabolites were detected in prophase, metaphase, anaphase, and telophase, respectively (Figure 1E). The distribution was significantly smaller from anaphase to telophase (Figure 1E). In plants, the formation and expansion of the cell plate depends on the phragmoplast and secretory vesicles, mostly derived from the trans-Golgi network (TGN), carrying material for the new cell plate to the division plane in anaphase (Samuels et al., 1995; Staelin and Hepler, 1996; Verma and Gu, 1996; Jürgens, 2005). The high number of metabolites in anaphase of negative mode can be explained by the new cell plate, necessitating increased trafficking from the Golgi and TGN or ER to the new plasma membrane.

VLCFAs are essential for cell plate formation during cytokinesis (Bach et al., 2011). This indicates that VLCFAs production increases in preparation for cytokinesis. To test this, we matched previously identified VLCFAs from the literature (Bach et al., 2011) in our dataset. Then, the median intensity of each VLCFA was plotted in a parallel coordinators plot (Figure 1F) to monitor the change of their abundance across the four cellular states. We found 17 lipids in our dataset, and out of which 15 had elevated levels in anaphase and telophase. Among them, the slope gradient of intensity was substantially increased in anaphase for C24:1 and in telophase for PE36:2 and PE36:3.

Furthermore, we examined whether a change in the metabolic profile occurs when the chromosome progression of mitosis is paused by a microtubule assembly inhibitor, propyzamide (Nagata et al., 1992; Akashi et al., 1988). Treatment with 3-μM propyzamide stops BY-2 cells from entering metaphase (Scaglia et al., 2014). BY-HR protoplasts were prepared after propyzamide treatment for 3 h. There were few differences in the cell phenotype and chromosome architecture in prometaphase between propyzamide-treated and dimethyl sulfoxide (DMSO)-treated control cells (Figure 2A). In the DMSO-treated group, prophase, prometaphase, metaphase, anaphase, and telophase cells were observed. However, in the propyzamide-treated group, only prophase and prometaphase cells were observed. Similar to the findings reported by Akashi et al. (1988), ∼20% of the protoplasts in the propyzamide-treated group showed scattered chromosomes throughout the cytoplasm (Figure 2A). Cell phase was classified after 3.5 h of treatment with propyzamide (Figure 2B). Cells showing the scattered chromosomes were defined as abnormal cells. We judged prometaphase cells as those in which the nuclear body was not visible, chromosome condensation was noticeable, and the chromosomes remained in the nuclear region and were not dispersed in the cytoplasm (Figure 2A). Prometaphase cells were 1.5% and 1.8% of the total cells treated with DMSO and propyzamide, respectively (Figure 2B). We isolated these cells, and analyzed by LSC-MS. A heatmap and principal component analysis-discriminant analysis (PCA-DA) plots of statistically significant peaks showed that there was a clear difference in metabolite profiles of a prometaphase cell between the propyzamide-treated and DMSO-treated groups (Figure 2C; Supplemental Figure S4; Supplemental Data Set 3). Whole metabolites showed a smaller distribution in the group treated with propyzamide (Figure 2D). In VLCFAs corresponding to *m/z* 339–910, the propyzamide-treated group showed wide distribution compared to the control group (Figure 2E). The action of propyzamide inhibits microtubule polymerization, suggesting that it causes changes in cell metabolites in addition to arresting chromosome migration. This result implies that the

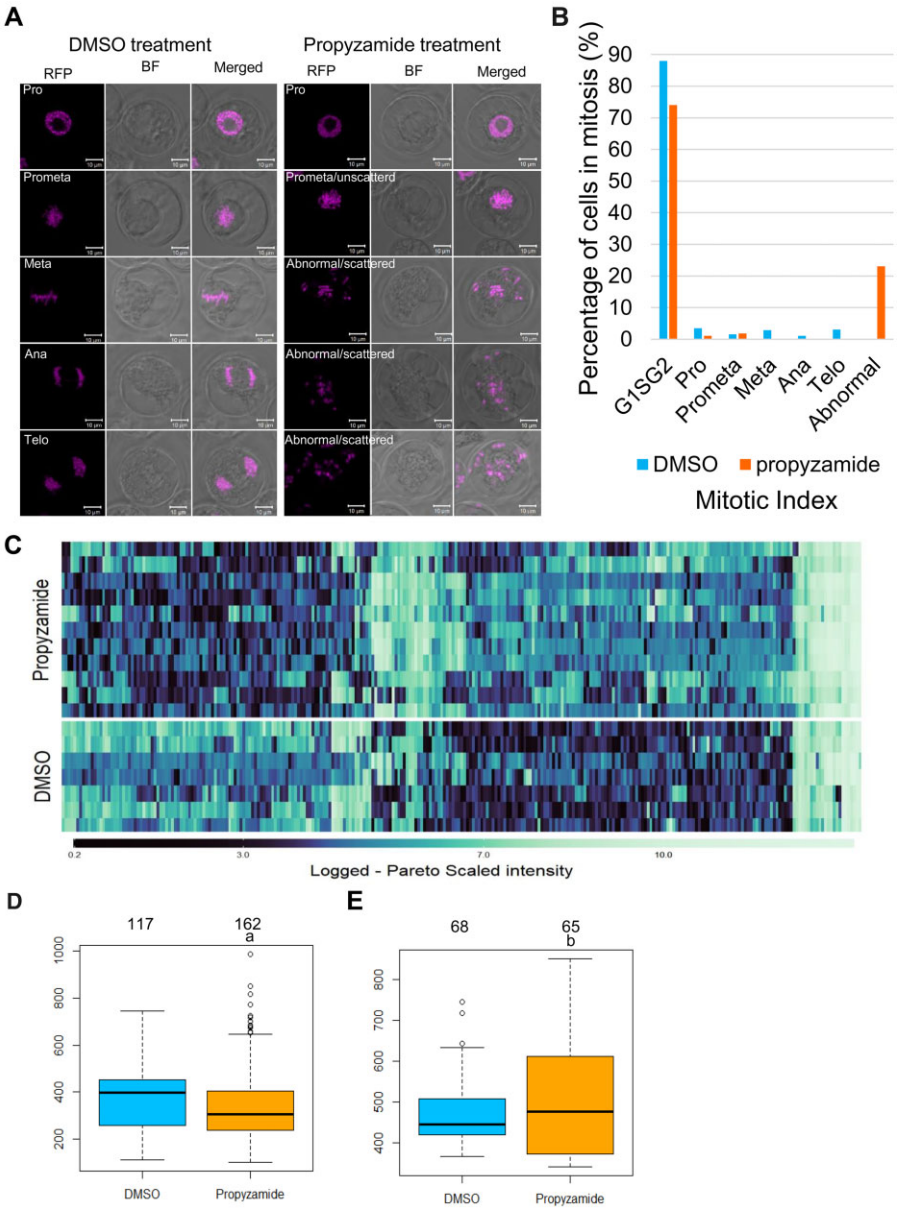

Figure 2 Changes in intracellular metabolites during the arrest of cell cycle progression by propyzamide. A, Effect of propyzamide treatment on mitotic BY-HR cells. Cells were incubated with 3 μM propyzamide or 0.1% DMSO as a control. Bars: 10 μm. B, Classification of chromosome status after treatment with propyzamide for 3 h. Cells whose chromosomes were scattered inside the cell are defined as unclassified. C, A heatmap shows significant peaks (Welch *t* test, $P < 0.05$) of propyzamide-treated cells and DMSO-treated (control) cells after a 3-h treatment. The rows show the metabolites and each column indicates a single cell. The colors correspond to the relative metabolite areas. Distribution of propyzamide-specific peaks in prometaphase cells of (D) all metabolites and (E) VLCFAs corresponding to *m*/*z* 339–910 in negative mode. Asterisks indicate a significant difference in distribution between the controls and the propyzamide-treated groups. The lower end of the whiskers shows the minimum value and the upper end of the whiskers shows the maximum value. The lower bottom of the box represents the 25 percentile of data from the smallest, the horizontal line in the box the median and the upper bottom the 75th percentile. Some of the points are outliers. The number shown above the box and whisker diagrams is the number of time-specific metabolites. $P < 0.03$ (*t* test).

synthesis of metabolites is occurring even under propyzamide treatment because high *m*/*z* lipids, such as VLCFAs, accumulate even if the mitosis is stopped for 3 h.

In this research, metabolic features were extracted by visualizing the sub-phases of mitosis and analyzing a wide range of metabolites at the single-cell level (Figure 1). This challenging approach has provided clues to the relationship between cell division progression and metabolite accumulation. In anaphase, larger phase-specific lipids accumulated, which suggest that lipids are synthesized in the transition from metaphase to anaphase for the formation of the new cell membrane and cell plate in preparation for their insertion in telophase. Bach et al. (2011) reported that a VLCFA-reducing Arabidopsis (*Arabidopsis thaliana*) mutant

(*pasticcino 2*) had a slower cell plate formation rate than that of wild-type, and the formation of the endomembrane tubular network was altered. This is supported by the accumulation of VLCFAs that was detected in anaphase, corroborating that VLCFAs promote cell plate formation. A substantial decrease in VLCFAs was observed from anaphase to telophase (Figure 1E) during which the phragmoplast is dismantled and the cell wall expands. It is speculated that the sharp reduction of VLCFAs in telophase is one of the events necessary for normal entry into cytokinesis.

We have shown the potential of single-cell analysis to study the metabolic profiles of plant mitotic sub-phases and revealed metabolic differences between the four mitotic sub-phases using BY-HR cells. Propyzamide arrests the cell cycle at metaphase, but previously nothing was known about how the cell contents are altered. Single-cell analysis of prometaphase cells treated with DMSO or propyzamide shows apparent differences in their metabolite profiles (Figure 2C). Inhibition of microtubule polymerization by propyzamide caused changes in VLCFA metabolism (Figure 2E). Even if microtubules are not formed after treatment with propyzamide and the cell cycle is arrested at prometaphase, high molecular weight lipids of *m/z* 339–910 accumulate. This indicates that the appearance of microtubule structures is not necessarily associated with the cellular metabolism. However, the fact that VLCFA-accumulated cells do not form cell plates under propyzamide means that lipid metabolization might proceed independently of cell mitosis.

This research provides a step in dissecting the intercellular contents of each mitotic sub-phase and understanding their roles in plant cell mitosis. The composition of lipids may have an important role in the progression of mitosis, and detailed verification of this will be necessary for the future.

Supplemental data

The following materials are available in the online version of this article.

Supplemental Figure S1. Establishment of BY-HR cells.

Supplemental Figure S2. Schematic diagram from single-cell acquisition to analysis.

Supplemental Figure S3. Heatmap visualization of significant peaks (analysis of variance (ANOVA) with post-hoc Tukey's HSD, $P < 0.05$) of all metabolites during mitotic progression.

Supplemental Figure S4. PCA-DA analysis of statistically significant peaks of propyzamide treatment group and DMSO prometaphase single cell.

Supplemental Table S1. Annotated list of phase-specific metabolites for positive mode measurements.

Supplemental Table S2. Annotated list of phase-specific metabolites for negative mode measurements.

Supplemental Data Set 1. Candidate molecules of phase-specific metabolites in positive mode.

Supplemental Data Set 2. Candidate molecules of phase-specific metabolites in negative mode.

Supplemental Data Set 3. Metabolite accumulation by propyzamide treatment.

Supplemental Materials and Methods.

Acknowledgments

The authors would like to thank Dr Takafumi Shimizu (NAIST Division of Biological Science) and Dr Mitsunori Seo (RIKEN Center for Sustainable Resource Science) for giving us an environment to continue our joint research. We also thank Dr Ryo Nakabayashi (RIKEN Center for Sustainable Resource Science), who gave us advice about the metabolome data analysis.

Funding

This study was supported by the Japan Society for the Promotion of Science (JSPS) KAKENHI [Grant-in-Aid for Challenging Exploratory Research (No.17K19363) to E.O.K.] and by RIKEN (the Single Cell Project to E.O.K and the Pioneering Project "Biology of Intracellular Environments" to Y.K and M. M").

Conflict of interest statement. None declared.

References

Abouleila Y, Onidani K, Ali A, Shoji H, Kawai T, Lim CT, Kumar V, Okaya S, Kato K, Hiyama E, et al. (2019) Live single cell mass spectrometry reveals cancer-specific metabolic profiles of circulating tumor cells. Cancer Sci **110**: 697–706

Afendi FM, Okada T, Yamazaki M, Hirai-Morita A, Nakamura Y, Nakamura K, Ikeda S, Takahashi H, Amin A, Darusman LK, et al. (2011) KNApSAcK family databases: integrated metabolite–plant species databases for multifaceted plant research. Plant Cell Physiol **53**: e1

Akashi T, Izumi K, Nagano E, Enomoto M, Mizuno K, Shibaoka H (1988) Effects of propyzamide on tobacco cell microtubules in vivo and in vitro. Plant and Cell Physiol **29:** 1053–1062

Alberts B, Bray A, Lewis J, Raff M, Roberts K, Watson JD (1994) Molecular Biology of the Cell, 3rd edn. Garland Publishing, New York, NY

Ali A, Abouleila Y, Shimizu Y, Hiyama E, Watanabe TM, Yanagida T, Germond A (2019) Single-cell screening of tamoxifen abundance and effect using mass spectrometry and Raman spectroscopy. Anal Chem **91:** 2710–2718

Atilla-Gokcumen GE, Muro E, Relat-Goberna J, Sasse S, Bedigian A, Coughlin ML, Garcia-Manyes S, Eggert US (2014) Dividing cells regulate their lipid composition and localization. Cell **156:** 428–439

Bach L, Gissot L, Marion J, Tellier F, Moreau P, Satiat-Jeunemaître B, Palauqui JC, Napier JA, Faure JD (2011) Very-long-chain fatty acids are required for cell plate formation during cytokinesis in *Arabidopsis thaliana*. J Cell Sci **124:** 3223–3234

Caillaud MC (2019) Anionic lipids: a pipeline connecting key players of plant cell division. Front Plant Sci **10:** 419

Fujii T, Matsuda S, Tejedor M, Esaki T, Sakane I, Mizuno H, Tsuyama N, Masujima T (2015) Direct metabolomics for plant cells by live single-cell mass spectrometry. Nat Protoc **10:** 1445–1456

Kihara A (2012) Very long-chain fatty acids: elongation, physiology and related disorders. J Biochem **152:** 387–395

Nagata T, Nemoto Y, Hasezawa S (1992) Tobacco BY-2 cell line as the "HeLa" cell in the cell biology of higher plants. Int Rev Cytol **132**: 1–30

Jürgens G (2005) Plant cytokinesis: fission by fusion. Trends Cell Biol **15:** 277–283

Samuels AL, Giddings TH, Staehelin LA (1995) Cytokinesis in tobacco BY-2 and root tip cells: a new model of cell plate formation in higher plants. J Cell Biol **130:** 1345–1357

Scaglia N, Tyekucheva S, Zadra G, Photopoulos C, Loda M (2014) De novo fatty acid synthesis at the mitotic exit is required to complete cellular division. Cell Cycle **13:** 859–868

Staelin LA, Hepler PK (1996) Cytokinesis in higher plants. Cell **84:** 821–824

Tejedor ML, Mizuno H, Tsuyama N, Harada T, Masujima T (2012) In situ molecular analysis of plant tissues by live single-cell mass spectrometry. Anal Chem **84:** 5221–5228

Verma DPS, Gu X (1996) Vesicle dynamics during cell plate formation in plants. Trends Plant Sci **1:** 145–149